Kaposi's sarcoma-associated herpesvirus ORF68 is a DNA binding protein required for viral genome cleavage and packaging

Matthew R Gardner[a], and Britt A Glaunsinger[a,b,c,#]

[a] Division of Infectious Diseases and Immunity, School of Public Health, University of California Berkeley, CA, USA

[b] Department of Plant & Microbial Biology, University of California Berkeley, CA, USA

[c] Howard Hughes Medical Institute, Chevy Chase, MD, USA

[#]Corresponding Author: glaunsinger@berkeley.edu

Running title: KSHV ORF68 is essential for genome encapsidation

Abstract

Herpesviral DNA packaging into nascent capsids requires multiple conserved viral proteins that coordinate genome encapsidation. Here, we investigated the role of the ORF68 protein of Kaposi's sarcoma-associated herpesvirus (KSHV), a protein required for viral DNA encapsidation whose function remains largely unresolved across the herpesviridae. We found that KSHV ORF68 is expressed with early kinetics and localizes predominantly to viral replication compartments, although it is dispensable for viral DNA replication and gene expression. However, in agreement with its proposed role in viral DNA packaging, KSHV-infected cells lacking ORF68 failed to cleave viral DNA concatemers, accumulated exclusively immature B-capsids, and released no infectious progeny virions. ORF68 has no predicted domains aside from a series of putative zinc finger motifs. However, *in vitro* biochemical analyses of purified

ORF68 protein revealed that it robustly binds DNA and is associated with nuclease activity. These activities provide new insights into the role of KSHV ORF68 in viral genome encapsidation.

Importance

Kaposi's sarcoma-associated herpesvirus (KSHV) is the etiologic agent of Kaposi's sarcoma and several B-cell cancers, causing significant morbidity and mortality in immunocompromised individuals. A critical step in the production of infectious viral progeny is the packaging of the newly replicated viral DNA genome into the capsid, which involves coordination between at least seven herpesviral proteins. While the majority of these packaging factors have been well studied in related herpesviruses, the role of the KSHV ORF68 protein and its homologs remains unresolved. Here, using a KSHV mutant lacking ORF68, we confirm its requirement for viral DNA processing and packaging in infected cells. Furthermore, we show that the purified ORF68 protein directly binds DNA and is associated with a metal-dependent cleavage activity on double stranded DNA *in vitro*. These activities suggest a novel role for ORF68 in herpesviral genome processing and encapsidation.

Introduction

Herpesviruses are large, double-stranded DNA viruses with complex virion assembly and maturation strategies. Following the expression of structural genes, capsids are assembled in the nucleus, first through the production of fragile procapsids (1). Procapsids are formed by the binding and orientation of capsid proteins onto a protein scaffold, which is subsequently

45 digested by the viral protease, allowing further maturation into A-, B-, or C-capsids. A-capsids
46 lack both the protein scaffold and DNA genome and most likely arise from failed packaging
47 events (2). B-capsids retain the cleaved protein scaffold and may represent a DNA-packaging
48 failure, like A-capsids, or simply represent capsids that have not yet encountered the DNA-
49 packaging machinery. Successful packaging of the viral genome, which displaces the digested
50 scaffold proteins, results in the mature, DNA-containing C-capsids (3).

51 The process of viral DNA replication generates head-to-tail concatemers, which are
52 cleaved into unit-length genomes as they are packaged into immature capsids. In alpha and
53 betaherpesviruses, DNA packaging is coordinated by seven viral proteins, each of which is
54 essential for both cleavage and packaging of the newly replicated genomes (4). The proteins
55 required for DNA packaging have been most extensively studied in the alphaherpesvirus Herpes
56 Simplex virus type 1 (HSV-1), where the essential proteins are UL6, UL15, UL17, UL25, UL28,
57 UL32, and UL33. UL6 forms a ring-shaped oligomer, which occupies one vertex of the
58 icosahedral capsid, forming the portal through which the DNA is threaded during both
59 packaging and unpackaging (5). UL28, UL15, and UL33 form the terminase motor, an ATP-
60 dependent motor that physically threads the viral genome through the portal complex into the
61 nascent capsid (6). Of the terminase motor, only UL28 has been shown to directly bind DNA (7).
62 However, UL15 and its homolog UL89 in betaherpesviruses have been shown to nick DNA
63 substrates *in vitro* (4, 8). UL17 and UL25 are part of the vertex-specific complex, which binds to
64 the vertices of the assembled capsid, as well as to the portal complex, thereby aiding docking of
65 the terminase motor (9, 10). UL32 is the only protein that is required for DNA cleavage and
66 packaging that lacks a well-defined function (4). However, UL32 contains a number of putative

67 C-X-X-C type zinc finger domains and mutation of these conserved motifs results in altered di-
68 sulfide patterns on the viral protease, which is involved in capsid assembly, supporting a role
69 for UL32 in viral genome encapsidation (11).

70 Significantly less is known about the DNA packaging process in gammaherpesviruses
71 such as Kaposi's sarcoma-associated herpesvirus (KSHV), although each of the packaging
72 proteins described above are conserved. These include KSHV ORF7 (UL28; terminase subunit),
73 ORF19 (UL25; vertex-specific complex), ORF29 (UL15; terminase subunit), ORF32 (UL17; vertex-
74 specific complex), ORF43 (UL6; portal protein), ORF67.5 (UL33; terminase subunit), and ORF68
75 (UL32; unknown). Cryo-electron microscopy of KSHV capsids indicated that KSHV ORF43 forms
76 the portal complex and that ORF32 is associated with vertices, consistent with studies in HSV-1
77 (12, 13).

78 Given that role ORF68 and its homologs play during viral DNA packaging are largely
79 unresolved across the herpesviridae, we sought to explore its function in more detail in KSHV-
80 infected cells and *in vitro*. During lytic KSHV infection, many features of ORF68 were conserved
81 with its alpha and betaherpesvirus homologs, such as localization to viral replication
82 compartments, and its requirement for viral genome cleavage, packaging, and infectious virion
83 production. Interestingly, biochemical analyses of recombinant ORF68 protein purified from
84 mammalian cells revealed it to be a DNA-binding protein that is associated with dsDNA
85 cleavage activity. These novel findings suggest that ORF68 plays a previously unappreciated role
86 in KSHV genome processing and encapsidation.

87

88 **Results**

89

90 **KSHV ORF68 is an early viral protein that localizes to viral replication compartments**

91 Although KSHV ORF68 has not been characterized, its homologs in alpha and
92 betaherpesviruses are expressed with late kinetics and are involved in viral DNA packaging (11,
93 14). ORF68 shares 24.8% sequence identity with UL32, its best characterized homolog from
94 HSV-1, including the five C-X-X-C motifs conserved across all the subfamily homologs (11). To
95 characterize the expression kinetics and potential functions of KSHV ORF68, we generated a
96 rabbit polyclonal antibody using recombinant ORF68 protein. We monitored the expression of
97 ORF68 in KSHV-infected iSLK.BAC16 cells, a commonly used Caki-1 cell line containing a
98 doxycycline (dox)-inducible version of the major viral lytic transactivator, ORF50 (RTA) (15, 16).
99 Lytic reactivation of these cells upon dox treatment revealed that ORF68 expression begins as
100 early as 6 hours post-reactivation and it is robustly expressed by 18 hours (Figure 1a). Its
101 expression kinetics mimicked those of the KSHV delayed early protein ORF59, and it was not
102 impacted by treatment with the viral DNA replication inhibitor phosphonoacetic acid (PAA),
103 which blocks expression of viral late genes such as K8.1 (Figure 1a). Thus, KSHV ORF68 is a
104 delayed early gene.

105 ORF68 has been alternatively annotated as a 467 amino acid (aa) protein and as a
106 longer, 545 aa protein containing a 78 aa N-terminal extension (ORF68-Extended) (Figure 1c).
107 However, on a western blot of iSLK.BAC16 lysate, ORF68 migrated as a single band at the
108 predicted molecular weight (MW) of the 467 aa form (52kDa). To confirm that the 467 aa
109 version was the expressed form in KSHV-infected cells, we cloned both versions into a
110 mammalian expression vector and compared their migration pattern in transfected HEK293T

111 cells to endogenous ORF68 in lytically-reactivated iSLK.BAC16 cells and the KSHV-infected B cell
112 line TREx-BCBL1. Indeed, in both cell lines, only the 467 aa form of ORF68 was detected (Figure
113 1b).

114 We next evaluated the subcellular localization of ORF68 in reactivated iSLK.BAC16 and
115 TREx-BCBL1 cells using immunofluorescence assays with the ORF68 antibody. To identify
116 infected cells, cells were co-stained with an antibody against the viral polymerase processivity
117 factor ORF59, which accumulates in viral replication compartments in the nucleus (17). We
118 observed no ORF68 staining in unreactivated or ORF59-negative cells, but in reactivated cells
119 ORF68 was present in both the cytoplasm and, more prominently, in the nucleus. In the
120 cytoplasm, it was primarily diffuse, but also localized to some randomly distributed puncta and
121 larger aggregates close to the nucleus. In the nucleus, ORF68 was localized predominantly in
122 viral replication compartments (Figure 2).

123

124 **KSHV lacking ORF68 maintains viral DNA replication and late gene expression, but does not**
125 **produce infectious virions**

126 To evaluate the role of ORF68 in the viral replication cycle, we generated an ORF68-
127 deficient virus (ORF68^{PTC}) using the BAC16 Red Recombinase system (15) by inserting two
128 premature termination codons 15 nt downstream of the translation start site. This virus was
129 used to establish a latently-infected cell line in iSLK cells. To ensure that any observed
130 phenotypes were not due to secondary mutations, we also engineered the corresponding
131 mutant rescue virus (ORF68^{PTC}-MR) (Figure 3a). Despite lacking ORF68 protein, the ORF68^{PTC}
132 virus expressed both the delayed early protein ORF59 and the late protein K8.1 at levels similar

133 to both the unmodified WT BAC16 KHSV and the ORF68^{PTC}-MR virus (Figure 3b). Furthermore,
134 qPCR analyses of viral DNA revealed no significant difference in DNA replication between any of
135 the viruses (Figure 3c). We then monitored production of infectious progeny virions using a
136 supernatant transfer assay, in which the supernatant from reactivated infected iSLK cells is
137 filtered and transferred to target cells. Because the BAC16-derived KSHV contains a virally-
138 encoded, constitutively-expressed GFP reporter gene, infected recipient cells can be quantified
139 by GFP expression using flow cytometry. Here, ORF68^{PTC} showed a marked defect, as no virus
140 production was detectable, while both WT and ORF68^{PTC}-MR infected cells produced sufficient
141 virus to infect nearly 100% of target cells (Figure 3d). Collectively, these data indicate that KSHV
142 ORF68 is essential for a late stage event in the viral replication cycle.
143
144 **In the absence of ORF68, KSHV DNA is not cleaved after replication**
145 The above results, together with studies of alpha and betaherpesvirus ORF68 homologs
146 (11, 14), suggested a role for KSHV ORF68 in viral DNA encapsidation. We therefore established
147 an assay similar to what has been used in other herpesviruses to measure packaging-associated
148 KSHV DNA cleavage, which occurs within the 801 bp GC-rich terminal repeat (TR) sequences
149 present in 20 – 40 tandem copies in the KSHV genome (18) (Figure 4a). Briefly, DNA was
150 isolated from infected iSLK cells and the TR sequences were released by digesting the DNA with
151 PstI-HF, which cleaves frequently within viral (and host) DNA, but not within the KSHV TRs. This
152 should generate a ladder of TR sequences, representing the collection of individual cleavage
153 events in the TRs that occur during packaging, which can be visualized by Southern blotting
154 with a DIG-labeled TR probe. As expected, we observed a robust increase in the high MW

155 uncleaved TRs following lytic reactivation of each sample, indicative of viral genome replication
156 (Figure 4b). However, DNA from ORF68^{PTC} infected cells showed no evidence of TR cleavage,
157 unlike DNA from WT and ORF68^{PTC}-MR infected cells, which displayed the expected laddering
158 phenotype (Figure 4b).
159
160 **KSHV ORF68^{PTC} accumulates exclusively B-capsids**
161 During herpesvirus assembly, immature procapsids are initially formed that contain
162 internal scaffolding proteins, which are subsequently proteolytically cleaved and extruded
163 during the process of DNA packaging (19, 20). This process yields mature, DNA-containing C-
164 capsids, but in the case of unsuccessful DNA packaging, either empty A-capsids or scaffold-
165 containing B-capsids are formed (3). To visualize the contribution of ORF68 towards capsid
166 maturation, we performed transmission electron microscopy on fixed samples of lytically-
167 reactivated iSLK cells containing either WT or ORF68^{PTC} KSHV. In the nuclei of WT KSHV infected
168 cells, we observed A, B, and C capsids (Figure 5a, b). In contrast, ORF68^{PTC} infected cells
169 contained exclusively B capsids (Figure 5a, b), indicating that KSHV DNA packaging is not
170 initiated in the absence of ORF68.
171
172 **ORF68 binds DNA with high affinity *in vitro* and is associated with metal-dependent nuclease**
173 **activity**
174 In order to study the biochemical activity of ORF68 as it relates to DNA packaging, we
175 sought to generate pure ORF68 protein. Our attempts to isolate recombinant ORF68 from *E.*
176 *coli* bacteria, *Pichia pastoris* yeast, and *SF9* insect cells did not yield properly folded protein

177 (data not shown). Thus, we instead purified TwinStrep-tagged ORF68 from transiently
178 transfected HEK293T cells by binding to Strep-TactinXT resin, followed by separation of ORF68
179 from the TwinStrep tag by PreScission protease cleavage and subsequent size exclusion
180 chromatography (Figure 6a). Mass spectrometry of the purified sample detected ORF68 but no
181 other contaminating proteins (data not shown). Notably, ORF68 eluted from gel filtration
182 columns as a ~275 kDa oligomer (based on injected standards) rather than as a monomer
183 (Figure 6b).

184 Given the failed DNA cleavage and packaging phenotypes associated with the ORF68^{PTC}
185 virus, we hypothesized that ORF68 might directly bind the viral genome to help direct DNA
186 packaging. We therefore used electrophoretic mobility shift assays (EMSA) to monitor binding
187 of purified ORF68 to a DNA probe containing the sequence of the KSHV TR *in vitro*. Indeed,
188 ORF68 efficiently bound DNA with an apparent K_d of (53.34 ± 2.11) nM (Figure 7a, b). The
189 binding was cooperative, with a Hill coefficient of 1.88 ± 0.12 (Figure 7b). This is comparable to
190 the 72 nM K_d of KSHV LANA binding to the terminal repeat (21). Multiple higher-order binding
191 events occurred at increased protein concentrations, resulting in several discrete bands of
192 protein-bound DNA (Figure 7a). Although this *in vitro* DNA-binding is robust, it does not appear
193 to be specific, as similar length probes of varying GC content from disparate sources were
194 bound with similar affinity, and also displayed higher order binding events (data not shown).

195 ORF68 has no identifiable domains aside from several predicted zinc finger motifs that
196 appear to be important for the structural integrity of the protein (22). However, we noted that
197 in the presence of Mg^{2+}, the TR probe or other circular or linear plasmid DNA was degraded
198 upon incubation with ORF68, suggesting that it may possess nuclease activity (Figure 7c, data

199 not shown). Nuclease activity required metal ions for catalysis, with a preference for Mg^{2+} or
200 Mn^{2+}, drastically reduced activity with Co^{2+} or Ni^{2+}, and no activity with Ca^{2+} or Zn^{2+} (Figure 7d).
201 Reactions were sensitive to EDTA or similar metal-chelating agents, consistent with our
202 observations that EDTA-containing buffers caused the precipitation of ORF68. Although our
203 mass spectrometry analysis of purified ORF68 did not detect contaminating peptides, at
204 present we cannot formally rule out the possibility that trace levels of a cellular nuclease co-
205 purified with ORF68, rather than nuclease activity being an intrinsic feature of ORF68. However,
206 given that ORF68 contains putative zinc finger motifs, we reasoned that in addition to inhibition
207 by EDTA, the associated nuclease activity should be sensitive to the zinc-specific chelator
208 N,N,N′,N′-tetrakis(2-pyridinylmethyl)-1,2-ethanediamine (TPEN), which has high affinity for Zn^{2+}
209 (K_d= 2.6 x 10^{-16} M), but very low affinity for Mg^{2+} (K_d= 2.6 x 10^{-2} M) and other divalent cations
210 (23-25). Indeed, the addition of TPEN prevented degradation of DNA in the presence of ORF68,
211 but not DNase I, a nuclease that requires Mg^{2+} for catalysis but does not contain any structural
212 zinc (Figure 7e). Collectively, these data demonstrate that KSHV ORF68 is a zinc finger-
213 containing protein that can bind DNA and is associated with a zinc-dependent DNase activity.
214
215 **Discussion**
216
217 Our data firmly establish that KSHV ORF68 is essential for genome encapsidation in
218 infected cells, and further suggest novel roles for purified ORF68 protein in DNA binding and
219 cleavage. This is the first demonstration of direct DNA binding by a DNA packaging-associated
220 protein in gammaherpesviruses, and the ORF68-associated nuclease activity suggests a

221 previously unappreciated function for this protein, which may relate to viral genome processing
222 and encapsidation. Such a role would be consistent with the defects in viral TR cleavage, DNA
223 packaging, and infectious virion formation we observed in cells infected with the ORF68^{PTC}
224 virus. It is further supported by our TEM analysis of infected cells, which showed that in the
225 absence of ORF68, DNA encapsidation was not initiated, as evidenced by the absence of A- and
226 C-capsids. Finally, our data are in line with phenotypes observed upon deletion of the ORF68
227 homologs in HSV-1 (11), HCMV (14) and Epstein-Barr virus (EBV) (26). Indeed, in EBV, deletion
228 of this BFLF1 gene was used to generate defective viral particles for use in vaccine development
229 (26).

230 The ORF68 homolog in HSV-1 (UL32) was recently shown to be involved in modulation of
231 disulfide bond formation during procapsid formation, which requires the presence of the
232 conserved C-X-X-C motifs (11). Deletion of individual cysteines within four of the five motifs
233 prevented complementation of a UL32 deletion mutant virus, and in the absence of UL32 the
234 disulfide bond profiles of other viral proteins were altered. In ORF68, however, the C-X-X-C
235 motifs appear to be important for its structural integrity, as chelation of Zn^{2+} causes ORF68 to
236 precipitate during purification in a manner that suggests unfolding (unpublished observations).
237 Thus, an important future challenge will be to resolve if these two functions are related, or if
238 specific roles for UL32 and ORF68 have diverged between the alpha- and gammaherpesviruses.

239 In the KSHV episome, the terminal repeats are present as 20 to 40 copies of a highly
240 repetitive ~800bp, 85% GC sequence (27). Unlike related herpesviruses, the packaging and
241 cleavage signals in the KSHV terminal repeats are unknown. However, by using a probe
242 generated from the entire repeat we could capture terminal repeats of any length. In a WT

243 KSHV infection, this yields a ladder-like cleavage pattern reflective of the fact that the genome
244 is replicated as head-to-tail concatemers, separated by an arbitrary number of terminal repeats.
245 While each genome should be cut only once at each end during packaging, the specific number
246 of repeats left at each genome terminus is variable (28, 29). This is in contrast to viruses lacking
247 ORF68, which displayed WT levels of DNA replication by both qPCR and Southern blotting, but
248 no apparent resolution of the amplified concatemers into unit-length genomes. These data
249 reinforce the hypothesis that KSHV ORF68 is not required for genome replication but is integral
250 to the process of DNA encapsidation. Interestingly, a recent cryo-electron microscopy (cryoEM)
251 structure of the HSV-1 portal-vertex shows a pentameric assembly associated with the portal
252 complex (30). Given that KSHV ORF68 purifies as an oligomer that is roughly the size of a
253 pentamer, one possibility it that this cryoEM-visualized pentameric assembly may serve as an
254 interaction site for ORF68 during the DNA packaging reaction.

255 Given the stage at which ORF68^{PTC} virus fails during virion maturation, we hypothesized
256 that ORF68 may interact with the viral genome to promote DNA packaging. Indeed, purified
257 ORF68 robustly bound the prototypical terminal repeat subunit, with an observed K_d of ~50nM.
258 This is comparable to the strength of the TR interaction for the KSHV latency-associated
259 episome tethering protein LANA, strongly suggesting that viral DNA binding is a biologically
260 relevant feature of ORF68 (21). However, it is important to note that *in vitro*, the DNA binding
261 activity of ORF68 does not have apparent sequence specificity. In cells, it is possible that
262 sequence specificity is conferred by other viral (or cellular) factors. It is also possible that the
263 DNA binding activity participates in a distinct facet of the viral lifecycle, although we did not
264 detect any defects in the ORF68^{PTC} virus prior to encapsidation. The ~800bp terminal repeat

265 subunits are somewhat long for traditional EMSA probes and as such, multiple binding events
266 could be observed. Furthermore, binding of ORF68 to DNA was cooperative, as is frequently
267 observed for DNA binding proteins (31). This cooperativity may indicate that ORF68 binds the
268 DNA probe at multiple sites, that the binding of the first ORF68 molecule alters the DNA
269 conformation in a way that promotes additional ORF68 binding, or simply reflect our
270 observation that ORF68 exists as an oligomer in solution.

271 In addition to DNA binding, we made the unexpected observation that in the presence
272 of the divalent cations Mg^{2+} or Mn^{2+}, incubation with ORF68 caused degradation of DNA. These
273 cations are commonly used by nucleases (32), and future studies are aimed at exploring
274 residues in ORF68 that could serve to coordinate divalent cations. Our robust purification
275 scheme, coupled with the absence of any detectable co-purifying peptides by mass
276 spectrometry and the fact that addition of the zinc-chelator TPEN specifically blocked ORF68-
277 associated nuclease activity suggest that the activity is intrinsic to ORF68. However, aside from
278 the zinc finger motifs, no predicted domains or structural information is currently available for
279 ORF68. Thus, a key challenge will be to establish if and how ORF68 promotes DNA cleavage in
280 cells. Formal proof of nuclease activity will ultimately require structural data to identify putative
281 catalytic domain(s), which should enable isolation of point mutants to be tested for DNA
282 cleavage. Similar to the DNA binding activity, our *in vitro* cleavage reactions do not capture TR-
283 specific targeting, as we found that other non-viral DNA was similarly susceptible to ORF68-
284 associated degradation (unpublished observations). This might suggest that other components
285 of the packaging machinery are required to confer specificity or, alternatively, that the putative
286 nuclease activity is involved in an ORF68 function independent of DNA encapsidation.

287 While seven herpesviral proteins are required for proper DNA encapsidation, only two
288 have been shown to directly act on DNA. A crystal structure of a fragment of the HSV-1 UL15
289 terminase motor protein, which is homologous to KSHV ORF29, revealed that it adopts an
290 RNase H-like fold and possess non-specific DNA nicking *in vitro* (8, 33). Purified HSV-1 UL28,
291 another terminase motor protein and the homolog of KSHV ORF7, has also been shown to bind
292 terminal repeat DNA *in vitro* (7). It has high specificity for certain terminal repeat DNA probes,
293 but only after heat treatment of the DNA, which causes them to adopt non-duplex structures
294 (7). This suggests that the UL28-DNA interaction is structure dependent, in contrast to KSHV
295 ORF68, which bound duplex DNA with no apparent sequence specificity or requirement for
296 higher order structures. Whether the UL15 and UL28 functions are conserved in their KSHV
297 homologs ORF29 and ORF7, and how KSHV ORF68 mechanistically contributes to DNA
298 encapsidation remain to be established.

299 Finally, although the majority of ORF68 is concentrated in replication compartments, the
300 protein also localizes within discrete puncta in the cytoplasm, as well as in larger aggregates
301 adjacent to the nucleus. While we hypothesize that the larger structures represent unfolded
302 protein in aggresomes, the smaller punctate structures are suggestive of a distinct function for
303 ORF68 in the cytoplasm, possibly unrelated to its role in packaging. Notably, HSV-1 UL32 was
304 also shown to localize to the cytoplasm, particularly late in infection, where it forms perinuclear
305 foci (11). Given the frequently multifunctional roles of viral proteins, it will be of interest to
306 explore possible additional cytoplasmic activities of ORF68.

307

308 **Methods**

309

310 **Plasmids**

311 TwinStrep-PreScission-ORF68 was cloned into the pHEK293 UltraExpression I vector
312 (Clontech) digested with XhoI and SalI. ORF68 was amplified with the primers 5'-
313 TGGAATTCTGCAGATATGTTTGTTCCCTGGCAACTCG-3' and 5'-
314 GCCACTGTGCTGGATTCAAGCGTACAAGTGTGACGTCT-3' while TwinStrep-PreScission was
315 amplified using the primers 5'-
316 CCTCCCCGGGCTCGAATGAGTGCGTGGAGTCATCCTCAATTCGAGAAAGGTG-3' and 5'-
317 GGGCCCCTGGAACAGAACTTCCAGTCCGGATTTTTCGAACTGCGGG-3'. The two fragments were
318 first assembled by PCR and then inserted into the vector by InFusion cloning (Clontech).

319 ORF68 and ORF68-Extended were cloned into pCDNA4 (ThermoFisher) digested with
320 EcoRV using 5'-TGGAATTCTGCAGATATGTTTGTTCCCTGGCAACTCG-3' for ORF68, 5'-
321 TGGAATTCTGCAGATATGTCACGAGGCAGAAGCTGG-3' for ORF68-Extended, and 5'-
322 GCCACTGTGCTGGATTCAAGCGTACAAGTGTGACGTCT-3' as the reverse primer for both. PCR
323 products were inserted into the vector using InFusion cloning.

324

325 **Cell Lines**

326 HEK293T (ATCC CRL-3216) cells were maintained in DMEM +10% FBS. HEK293T-ORF68
327 cells were maintained in DMEM + 10% FBS, 325 µg/ml zeocin. iSLK.BAC16 (15) cells were
328 maintained in DMEM + 10% FBS, 1 mg/ml hygromycin B, and 1 µg/ml puromycin. TREx-BCBL1
329 (34) cells were maintained in RPMI 1640 + 20% FBS.

330

331 **Viral mutagenesis and infection studies**

332 The KSHV ORF68 Premature Termination Codon (ORF68^{PTC}) mutant and corresponding
333 mutant rescue (MR) were engineered using the scarless Red recombination system in BAC16
334 GS1783 *E. coli* as previously described (15), except using two gBlocks (IDT) to introduce the
335 mutation. Each gBlock contained half of the kanamycin resistance cassette, as well as the
336 desired mutation, and were joined by short overlap extension PCR before being used as the
337 linear insert in the established protocol.

338 The BAC16 ORF68 mutant and MR were purified using the NucleoBond BAC 100 kit
339 (Clontech). iSLK cell lines latently infected with the KSHV ORF68^{PTC} virus were then established
340 by co-culture of the relevant BAC16-containing HEK293T cells with uninfected target iSLK-Puro
341 cells. HEK293T cells constitutively expressing ORF68 (HEK293T-ORF68) were transfected with 12
342 µg of BAC16 containing ORF68^{PTC} or MR using linear polyethylenimine (PEI, MW ~25,000) at a
343 1:3 DNA:PEI ratio. The following day, the cells were trypsinized and mixed 1:1 with iSLK-puro
344 cells, then treated with 30 nM 12-O-Tetradecanoylphorbol-13-acetate (TPA) and 300 nM
345 sodium butyrate for 4 days to induce lytic replication. Cells were then incubated with selection
346 media containing 300 µg/ml hygromycin B, 1 µg/ml puromycin, and 250 µg/ml G418. Media
347 was replaced every other day for ~2 weeks, gradually increasing the hygromycin B
348 concentration to 1 mg/ml until there were no HEK293T cells remaining and the iSLK cells were
349 green and replicating.

350 For induction studies, BAC16-containing iSLK cells were treated with 1 µg/ml doxycycline
351 and 1 mM sodium butyrate, and TREx-BCBL1 cells were induced with doxycycline (1 µg/ml) and
352 TPA (25 ng/ml) for the indicated amount of time. Virion production from reactivated iSLK cells

353 was measured using supernatant transfer assays at 72 hours post induction. The supernatant
354 was filtered through a 0.45 µM PES filter, then 2 ml were mixed with $1x10^6$ freshly trypsinized
355 HEK293T cells. The cell mixture was placed into a 6 well plate and centrifuged at 1,200 x *g* for 2
356 hours at 32˚C. The following day, cells were trypsinized, fixed in 4% paraformaldehyde, then
357 analyzed for GFP expression by flow cytometry (BD Csampler, BD Biosciences). Data was
358 analyzed using FlowJo v10.
359
360 **Generation of HEK293T cells stably expressing ORF68**
361 HEK293T-ORF68 cells were generated by cloning ORF68 into pLJM1 (a gift from David
362 Sabatini (Addgene plasmid #19319) (35)) in which the puromycin resistance had been
363 exchanged for zeocin. The vector was digested with AgeI and EcoRI (New England Biolabs) and
364 ORF68 was amplified by PCR using primers 5'-
365 CGCTAGCGCTACCGGATGTTTGTTCCCTGGCAACTCGG-3' and 5'-
366 TCGAGGTCGAGAATTTCAAGCGTACAAGTGTGACGTCTG-3' and inserted using T4 DNA Ligase
367 (NEB). 1.6 µg of this plasmid was co-transfected into HEK293T cells along with the lentiviral
368 packaging plasmids pMD2.G (0.5 µg) and psPAX2 (1.3 µg) (gifts from Didier Trono (Addgene
369 plasmid #12259 and #12260)) using PEI. 48 hours after transfection, the supernatants were
370 collected, filtered through a 0.45 µm PES filter, diluted 1:4 (supernatant:media) in serum-free
371 DMEM containing 8 µg/ml of polybrene, and added to the wells of a 6 well plate containing
372 $1x10^6$ HEK293T cells per well. The plates were centrifuged for 2 hours at 1,200 x *g* (32˚C),
373 incubated overnight, and the media replaced with fresh DMEM (10% FBS) containing 325 µg/ml
374 zeocin until no further cell death was observed, roughly two weeks.

375

376 **Western blots and antibody production**

377 Cells were lysed in protein lysis buffer (50 mM Tris-HCl pH 7.6, 150 mM NaCl, 3 mM
378 $MgCl_2$, 10% glycerol, 0.5% NP-40, cOmplete EDTA-free Protease Inhibitors [Roche]) and clarified
379 by centrifugation at 20,000 x *g* for 10 min at 4˚C. Lysates were resolved by SDS-PAGE and
380 western blotted with rabbit anti-ORF68 (1:5000), rabbit anti-ORF59 (1:10,000), rabbit anti-K8.1
381 (1:10,000), rabbit anti-histone H3 (1:3000, Cell Signaling 4499S), or mouse anti-GAPDH (1:5000,
382 Abcam ab8245). Rabbit anti-ORF68, -ORF59, and -K8.1 was produced by Pocono Rabbit Farm &
383 Laboratory by immunizing rabbits against MBP-ORF68, -ORF59, or -K8.1 (gifts of Denise Whitby,
384 (36)). Sera was harvested and used directly for ORF59 and K8.1, while ORF68-specific antibodies
385 were isolated by first collecting antibodies that bound an MBP-ORF68 column, followed by
386 removal of non-specific antibodies on an MBP column. Both selection columns were generated
387 using the AminoLink Plus Immobilization Kit (ThermoFisher).

388

389 **Immunofluorescence assays**

390 Cells were fixed with 4% paraformaldehyde, permeabilized with ice-cold methanol at -
391 20˚C for 20 min, then blocked with BSA blocking buffer (PBS, 1% Triton X-100, 0.5% Tween20,
392 3% BSA) for 30 minutes at room temperature. They were then incubated with rabbit anti-ORF68
393 and mouse anti-ORF59 (Advanced Biotechnologies) antibodies (diluted 1:100 in blocking buffer)
394 overnight at 4˚C, washed with PBS, and incubated with secondary antibody (AlexaFluor594 or
395 DyLight650, 1:1000 in BSA blocking buffer) for 1 h at 37˚C, and mounted using VectaShield

396 HardSet with DAPI (ThermoFisher). Images were acquired on an EVOS FL inverted fluorescent
397 microscope (ThermoFisher).
398
399 **DNA isolation and qPCR**
400 iSLK-BAC16 cells were incubated with 5x proteinase K digestion buffer (50 mM Tris-HCl
401 pH 7.4, 500 mM NaCl, 5 mM EDTA, 2.5% SDS) and digested with proteinase K (80 µg/ml)
402 overnight at 55˚C. The gDNA was isolated using Zymo Quick gDNA Miniprep Kit according to the
403 manufacturer's instructions.
404 Quantitative PCR was performed on the isolated DNA using iTaq Universal SYBR Green
405 Supermix on a QuantStudio3 Real-Time PCR machine. DNA levels were quantified using relative
406 standard curves with primers specific for KSHV ORF57 (5'-GGTGTGTCTGACGCCGTAAAG-3' and
407 5'-CCTGTCCGTAAACACCTCCG-3') or a region in the GAPDH promoter (5'-
408 TACTAGCGGTTTTACGGGCG-3' and 5'-TCGAACAGGAGGAGCAGAGAGCGA-3'). The relative
409 genome numbers were normalized to GAPDH to account for loading differences and to
410 uninduced samples to account for starting genome copy number.
411
412 **Protein purification**
413 TwinStrep-PreScission-ORF68 was transfected using PEI into 50 90% confluent 15 cm
414 plates of HEK293T cells for 48h. Cells were lysed in 5 ml of lysis buffer (100 mM Tris-HCl pH 8.0,
415 300 mM NaCl, 1 mM DTT, 5% glycerol, 0.1% CHAPS, 1 µg/ml avidin, cOmplete EDTA-free
416 protease inhibitors [Sigma-Aldrich]) per 1 g of cell pellet and rotated at 4˚C for an additional 30
417 minutes. The viscosity was reduced by sonication, whereupon debris was removed by

418 centrifugation at 20,000 x *g* (4˚C) for 30 min followed by filtration through a 0.45 µm PES filter
419 with a glass pre-filter (Millipore). Lysate was passed three times over a gravity column
420 containing Strep-Tactin XT Superflow slurry (IBA) then washed with 5 column volumes of strep
421 running buffer (100 mM Tris-HCl pH 8.0, 300 mM NaCl, 1 mM DTT, 5% glycerol, 0.1% CHAPS).
422 ORF68 was eluted by rotating the column overnight in HRV 3C Protease (Millipore) at a 1:100
423 Protease:ORF68 ratio in buffer containing 2 mM DTT, then concentrated to ~500 µL using a 30
424 kDa cut-off Centriprep spin concentrator (Millipore). The concentrated eluate was centrifuged
425 at 20,000 x *g* for 10 min to remove precipitates and injected onto a HiLoad 16/600 Superdex
426 200 pg gel filtration column (GE Healthcare), previously equilibrated with Gel Filtration buffer
427 (50 mM HEPES pH 7.6, 100 mM NaCl, 100 mM KCl, 5% glycerol, 0.1% CHAPS). Gel filtration was
428 performed using an AKTA Pure FPLC (GE Healthcare). Fractions resulting from the gel filtration
429 were analyzed by SDS-PAGE and staining with colloidal Coomassie (37). Fractions containing
430 ORF68 were pooled and concentrated as before, until the total concentration was ~2 mg/mL as
431 evaluated by absorbance at 280 nm. The concentrated protein was injected into a 20 kDa cut-
432 off Slide-A-Lyzer dialysis cassette (ThermoFisher) and dialyzed against storage buffer (Gel
433 Filtration buffer lacking CHAPS). Dialyzed protein was diluted to 1 mg/ml, aliquoted, and snap-
434 frozen in liquid nitrogen before being stored at -80˚C.
435
436 **Electrophoretic mobility shift assay**
437 Single-subunit terminal repeat DNA probes were generated by digesting pK8TR (a gift of
438 the Kaye lab (18)) with AscI overnight. The resulting cleavage products were separated on an

439 agarose gel and the 800bp band was excised, isolated from agarose, and purified further by
440 phenol:chloroform extraction and ethanol precipitation.

441 EMSA assays were assembled on ice in gel shift buffer (25 mM HEPES pH 7.6, 50 mM
442 NaCl, 50 mM KCl, 0.1 mg/ml BSA, 0.05% CHAPS, 10% glycerol) with 5 nM probe and 2-fold
443 dilutions of ORF68 ranging from 1.95 nM to 1000 nM. Once assembled, the reactions were
444 incubated at 30˚C for 30 minutes. Samples were directly loaded onto a 3.5% 29:1
445 polyacrylamide:bisacrylamide native gel containing 45 mM Tris-borate pH 8.3, 10% glycerol,
446 which was degassed thoroughly before polymerization. Samples were separated by
447 electrophoresis at 250V for 1 hour at 4˚C in pre-chilled 0.5X TB (45 mM Tris-borate pH 8.3). Tris-
448 borate buffer was used in lieu of TBE because ORF68 precipitates in the presence of EDTA. The
449 native polyacrylamide gel was cast to a final concentration of 0.5X Tris-borate, 10% glycerol,
450 and was degassed thoroughly before polymerization. Following the electrophoresis, the gel was
451 removed from the running cassette and stained with SYBRgold (ThermoFisher) in 0.5X TB for 30
452 minutes, rocking at room temperature and protected from light. Staining solution was removed
453 by briefly washing with fresh 0.5X TB and the gel was imaged on a ChemiDoc Touch (Bio-rad).
454 All bands were quantified using ImageLab v6.0 (Bio-rad) and percent bound probe was
455 determined by dividing shifted band intensity by the total intensity of all bands in that lane.
456 Binding curves were generated using Prism v7 (GraphPad) by non-linear regression fit using
457 least-squares. Shown data represents three technical replicates performed on different days.

458

459 **Nuclease assays**

460 The EMSA probe was also used for nuclease assays and was produced as described
461 above. Reactions were assembled in nuclease buffer (25 mM HEPES pH 7.6, 50 mM NaCl, 50
462 mM KCl, 0.1 mg/ml BSA, 2.5 mM $MgCl_2$) with 1 nM DNA probe and 2-fold dilutions of ORF68
463 ranging from 9.77 to 5000 nM. The reactions were incubated at 37˚C overnight. The following
464 day, reactions were quenched using stop buffer (4 M urea, 50 mM EDTA, 1 mM $CaCl_2$, 0.8 U
465 proteinase K [New England Biolabs], 1x Purple Loading dye [New England Biolabs]; final
466 concentrations) and incubating at room temperature for 30 minutes. The samples were then
467 loaded onto a denaturing polyacrylamide gel (8 M Urea, 4.5% 29:1 acrylamide:bisacrylamide,
468 90 mM Tris-borate pH 8.3, 2 mM EDTA, degassed before polymerization), which had been pre-
469 run at 200V for 30 minutes in 1X TBE to evenly heat the gel. The samples were separated at
470 200V for 45 minutes before being removed from the running cassette and stained with
471 SYBRgold in 1X TBE for 30 minutes at room temperature, protected from light. Gels were
472 visualized using a ChemiDoc Touch (Bio-Rad). Metal-dependence tests were performed as
473 described but changing the 2.5 mM $MgCl_2$ to the chloride salts of the indicated divalent cations.
474 TPEN-treatment was performed as described but protein was treated with either TPEN in 100%
475 ethanol (1 mM), mock treated with 100% ethanol, or EDTA (50 mM) for 10 minutes on ice prior
476 to adding the DNA substrate. DNaseI (New England Biolabs) was diluted to 0.02U in ORF68
477 storage buffer before addition to reactions.
478
479 **Southern blotting**
480 BAC16.iSLK cells were harvested in proteinase K digestion buffer and incubated
481 overnight with proteinase K (80 µg/ml). DNA was isolated by phenol:chloroform extraction and

482 ethanol precipitation, then resuspended in TE buffer. DNA (10 µg) was digested with PstI-HF
483 (New England Biolabs) overnight then separated by electrophoresis in a 0.7% agarose 1x TBE
484 gel stained with SYBRsafe. The DNA was transferred to a NYTRAN-N membrane (GE Healthcare)
485 by capillary action in 20x SSC overnight and crosslinked to the membrane in a StrataLinker 2400
486 (Stratagene) using the AutoUV setting.

487 The membrane was treated according to the DIG High Prime DNA Labeling and
488 Detection Starter Kit II (Roche) following the manufacturer's instructions. Briefly, the
489 membrane was hybridized at 42˚C in EasyHyb Buffer with a DIG-labeled linear terminal repeat
490 subunit derived from AscI (New England Biolabs) digested pK8TR, which was labeled according
491 to kit instructions. Following overnight hybridization, the membrane was washed twice with 2X
492 SSC (+0.1% SDS) at room temperature and then twice with 0.5X SSC (+0.1% SDS) at 68˚C. Using
493 supplied reagents, the blot was then blocked, incubated with anti-DIG-AP antibody, and
494 visualized on a ChemiDoc Touch (Bio-Rad).

495

496 **Electron microscopy**

497 iSLK.BAC16 WT or ORF68^{PTC}-infected cells were induced for 48 hours as described
498 above. Cells were washed once with PBS and fixed with 2% glutaraldehyde, 4%
499 paraformaldehyde in 100 mM sodium cacodylate buffer, pH 7.2 for 10 minutes at room
500 temperature. Fixative was removed and cells were scraped into 2% glutaraldehyde in 100 mM
501 sodium cacodylate buffer, pH 7.2 and evenly resuspended by pipetting. Cells were then washed
502 with 1% osmium tetroxide, 0.8% ferricyanide in 100 mM sodium cacodylate buffer, pH 7.2,
503 before being treated with 1% uranyl acetate and dehydrated with increasing concentrations of

504 acetone. Samples were then infiltrated and embedded in resin, from which 70 nm sections
505 were cut on a Reichert-Jung microtome. Sections were picked up on copper mesh grids coated
506 with 0.5% formvar, post-stained with uranyl acetate and lead citrate, and examined using an FEI
507 Tecnai 12 transmission electron microscope.
508

509 **Acknowledgements**

510 We thank all members of the Glaunsinger and Coscoy labs, in particular Angelica
511 Castañeda and Allison Didychuk, as well as Dr. Sandra Weller for their helpful suggestions and
512 critical reading of the manuscript. We also thank Reena Zalpuri and all of the staff at the
513 University of California Berkeley Electron Microscope Laboratory for advice and assistance in
514 electron microscopy sample preparation and data collection. B.G. is an investigator of the
515 Howard Hughes Medical Institute. This research was also supported by NIH R01AI122528 to
516 B.G.
517

518 **References**
519

520 1. **Rixon FJ**, **McNab D**. 1999. Packaging-competent capsids of a herpes simplex virus
521 temperature-sensitive mutant have properties similar to those of in vitro-assembled
522 procapsids. J Virol **73**:5714–5721.
523
524 2. **Booy FP**, **Newcomb WW**, **Trus BL**, **Brown JC**, **Baker TS**, **Steven AC**. 1991. Liquid-crystalline,
525 phage-like packing of encapsidated DNA in herpes simplex virus. Cell **64**:1007–1015.
526
527 3. **Tandon R**, **Mocarski E**, **Conway J**. 2015. The A, B, Cs of Herpesvirus Capsids. Viruses **7**:899–
528 914.
529
530 4. **Heming JD**, **Conway JF**, **Homa FL**. 2017. Herpesvirus Capsid Assembly and DNA Packaging,
531 pp. 119–142. *In* Cell Biology of Herpes Viruses, 5 ed. Springer International Publishing,
532 Cham.
533
534 5. **Cardone G**, **Winkler DC**, **Trus BL**, **Cheng N**, **Heuser JE**, **Newcomb WW**, **Brown JC**, **Steven AC**.
535 2007. Visualization of the herpes simplex virus portal in situ by cryo-electron tomography
536 **361**:426–434.
537
538 6. **Heming JD**, **Huffman JB**, **Jones LM**, **Homa FL**. 2013. Isolation and Characterization of the
539 Herpes Simplex Virus 1 Terminase Complex. J Virol **88**:225–236.
540
541 7. **Adelman K**, **Salmon B**, **Baines JD**. 2001. Herpes simplex virus DNA packaging sequences
542 adopt novel structures that are specifically recognized by a component of the cleavage and
543 packaging machinery. Proc Natl Acad Sci USA **98**:3086–3091.
544
545 8. **Selvarajan Sigamani S**, **Zhao H**, **Kamau YN**, **Baines JD**, **Tang L**. 2013. The Structure of the
546 Herpes Simplex Virus DNA-Packaging Terminase pUL15 Nuclease Domain Suggests an
547 Evolutionary Lineage among Eukaryotic and Prokaryotic Viruses. J Virol **87**:7140–7148.
548
549 9. **Thurlow JK**, **Murphy M**, **Stow ND**, **Preston VG**. 2006. Herpes Simplex Virus Type 1 DNA-
550 Packaging Protein UL17 Is Required for Efficient Binding of UL25 to Capsids. J Virol **80**:2118–
551 2126.
552
553 10. **Newcomb WW**, **Homa FL**, **Brown JC**. 2006. Herpes Simplex Virus Capsid Structure: DNA
554 Packaging Protein UL25 Is Located on the External Surface of the Capsid near the Vertices. J
555 Virol **80**:6286–6294.
556
557 11. **Albright BS**, **Kosinski A**, **Szczepaniak R**, **Cook EA**, **Stow ND**, **Conway JF**, **Weller SK**. 2014. The
558 Putative Herpes Simplex Virus 1 Chaperone Protein UL32 Modulates Disulfide Bond
559 Formation during Infection **89**:443–453.
560

561 12. **Deng B**, **O'Connor CM**, **Kedes DH**, **Zhou ZH**. 2008. Cryo-electron tomography of Kaposi's
562 sarcoma-associated herpesvirus capsids reveals dynamic scaffolding structures essential to
563 capsid assembly and maturation. Journal of Structural Biology **161**:419–427.
564
565 13. **Dai X**, **Gong D**, **Wu TT**, **Sun R**, **Zhou ZH**. 2014. Organization of Capsid-Associated Tegument
566 Components in Kaposi's Sarcoma-Associated Herpesvirus. J Virol **88**:12694–12702.
567
568 14. **Borst EM**, **Wagner K**, **Binz A**, **Sodeik B**, **Messerle M**. 2008. The Essential Human
569 Cytomegalovirus Gene UL52 Is Required for Cleavage-Packaging of the Viral Genome
570 **82**:2065–2078.
571
572 15. **Brulois KF**, **Chang H**, **Lee AS-Y**, **Ensser A**, **Wong L-Y**, **Toth Z**, **Lee SH**, **Lee H-R**, **Myoung J**,
573 **Ganem D**, **Oh T-K**, **Kim JF**, **Gao S-J**, **Jung JU**. 2012. Construction and Manipulation of a New
574 Kaposi's Sarcoma-Associated Herpesvirus Bacterial Artificial Chromosome Clone. J Virol
575 **86**:9708–9720.
576
577 16. **Myoung J**, **Ganem D**. 2011. Generation of a doxycycline-inducible KSHV producer cell line of
578 endothelial origin: Maintenance of tight latency with efficient reactivation upon induction.
579 Journal of Virological Methods **174**:12–21.
580
581 17. **Wu FY**, **Ahn JH**, **Alcendor DJ**, **Jang WJ**, **Xiao J**, **Hayward SD**, **Hayward GS**. 2001. Origin-
582 Independent Assembly of Kaposi's Sarcoma-Associated Herpesvirus DNA Replication
583 Compartments in Transient Cotransfection Assays and Association with the ORF-K8 Protein
584 and Cellular PML. J Virol **75**:1487–1506.
585
586 18. **Habison AC**, **de Miranda MP**, **Beauchemin C**, **Tan M**, **Cerqueira SA**, **Correia B**, **Ponnusamy**
587 **R**, **Usherwood EJ**, **McVey CE**, **Simas JP**, **Kaye KM**. 2017. Cross-species conservation of
588 episome maintenance provides a basis for in vivo investigation of Kaposi's sarcoma
589 herpesvirus LANA. PLoS Pathog **13**:e1006555–25.
590
591 19. **Gibson W**, **virology BRJO**, **1972**. Proteins specified by herpes simplex virus VIII.
592 Characterization and composition of multiple capsid forms of subtypes 1 and 2. Am Soc
593 Microbiol.
594
595 20. **Rixon FJ**, **Cross AM**, **Addison C**, **Preston VG**. 1988. The products of herpes simplex virus type
596 1 gene UL26 which are involved in DNA packaging are strongly associated with empty but
597 not with full capsids. Journal of General Virology **69 (Pt 11)**:2879–2891.
598
599 21. **Hellert J**, **Weidner-Glunde M**, **Krausze J**, **Lünsdorf H**, **Ritter C**, **Schulz TF**, **Lührs T**. 2015. The
600 3D structure of Kaposi sarcoma herpesvirus LANA C-terminal domain bound to DNA. Proc
601 Natl Acad Sci USA **112**:6694–6699.
602
603 22. **Chang YE**, **Poon AP**, **Roizman B**. 1996. Properties of the protein encoded by the UL32 open
604 reading frame of herpes simplex virus 1. J Virol **70**:3938–3946.

605
606 23. **Hyun HJ**, **Sohn JH**, **Ha DW**, **Ahn YH**, **Koh JY**, **Yoon YH**. 2001. Depletion of intracellular zinc
607 and copper with TPEN results in apoptosis of cultured human retinal pigment epithelial
608 cells. Invest Ophthalmol Vis Sci **42**:460–465.
609
610 24. **Arslan P**, **Di Virgilio F**, **Beltrame M**, **Biological RTJO**, **1985**. 1985. Cytosolic Ca2+ homeostasis
611 in Ehrlich and Yoshida carcinomas. A new, membrane-permeant chelator of heavy metals
612 reveals that these ascites tumor cell lines have …. ASBMB **260**:2719–2727.
613
614 25. **Golovine K**, **Uzzo RG**, **Makhov P**, **Crispen PL**, **Kunkle D**, **Kolenko VM**. 2008. Depletion of
615 intracellular zinc increases expression of tumorigenic cytokines VEGF, IL-6 and IL-8 in
616 prostate cancer cells via NF-κB-dependent pathway. Prostate **68**:1443–1449.
617
618 26. **Pavlova S**, **Feederle R**, **Gartner K**, **Fuchs W**, **Granzow H**, **Delecluse HJ**. 2013. An Epstein-Barr
619 Virus Mutant Produces Immunogenic Defective Particles Devoid of Viral DNA. J Virol
620 **87**:2011–2022.
621
622 27. **Juillard F**, **Tan M**, **Li S**, **Kaye KM**. 2016. Kaposi's Sarcoma Herpesvirus Genome Persistence
623 **7**:1883–1815.
624
625 28. **Varmuza SL**, **Smiley JR**. 1985. Signals for site-specific cleavage of HSV DNA: maturation
626 involves two separate cleavage events at sites distal to the recognition sequences. Cell
627 **41**:793–802.
628
629 29. **Tong L**, **Stow ND**. 2009. Analysis of Herpes Simplex Virus Type 1 DNA Packaging Signal
630 Mutations in the Context of the Viral Genome. J Virol **84**:321–329.
631
632 30. **McElwee M**, **Vijayakrishnan S**, **Rixon F**, **Bhella D**. 2018. Structure of the herpes-simplex
633 virus portal-vertex. bioRxiv https://doi.org/10.1101/290544.
634
635 31. **Siggers T**, **Gordan R**. 2014. Protein-DNA binding: complexities and multi-protein codes.
636 Nucleic Acids Res **42**:2099–2111.
637
638 32. **Yang W**. 2010. Nucleases: diversity of structure, function and mechanism. Quart Rev
639 Biophys **44**:1–93.
640
641 33. **Nadal M**, **Mas PJ**, **Blanco AG**, **Arnan C**, **Sola M**, **Hart DJ**, **Coll M**. 2010. Structure and
642 inhibition of herpesvirus DNA packaging terminase nuclease domain. Proc Natl Acad Sci USA
643 **107**:17059–17059.
644
645 34. **Nakamura H**, **Lu M**, **Gwack Y**, **Souvlis J**, **Zeichner SL**, **Jung JU**. 2003. Global Changes in
646 Kaposi's Sarcoma-Associated Virus Gene Expression Patterns following Expression of a
647 Tetracycline-Inducible Rta Transactivator. J Virol **77**:4205–4220.
648

649 35. **Sancak Y**, **Peterson TR**, **Shaul YD**, **Lindquist RA**, **Thoreen CC**, **Bar-Peled L**, **Sabatini DM**.
650 2008. The Rag GTPases Bind Raptor and Mediate Amino Acid Signaling to mTORC1. Science
651 **320**:1496–1501.
652
653 36. **Labo N**, **Miley W**, **Marshall V**, **Gillette W**, **Esposito D**, **Bess M**, **Turano A**, **Uldrick T**,
654 **Polizzotto MN**, **Wyvill KM**, **Bagni R**, **Yarchoan R**, **Whitby D**. 2014. Heterogeneity and
655 Breadth of Host Antibody Response to KSHV Infection Demonstrated by Systematic Analysis
656 of the KSHV Proteome. PLoS Pathog **10**:e1004046–11.
657
658 37. **Dyballa N**, **Metzger S**. 2009. Fast and Sensitive Colloidal Coomassie G-250 Staining for
659 Proteins in Polyacrylamide Gels. JoVE 1–5.
660

661 **Figure 1**

662 Characterization of the expression of KSHV ORF68. (A) Western blot showing the expression
663 kinetics of ORF68 relative to the early protein ORF59 and the late protein K8.1 in iSLK.BAC16
664 cells post reactivation with doxycycline (dox). GAPDH serves as a loading control. (B) Anti-
665 ORF68 western blot of lysates of HEK293T cells transfected with plasmids expressing either the
666 extended (ORF68-Extended) or shorter form of ORF68, next to lysates of lytically reactivated
667 iSLK.BAC16 and TREx-BCBL1 cells. Different amounts of lysate were loaded in each lane to
668 account for differing ORF68-expression levels. (C) Diagram showing the genomic locus of
669 ORF68, showing the two annotated forms, which differ by a 78 amino acid (aa) N-terminal
670 extension.

671

672 **Figure 2**

673 ORF68 localizes within replication compartments and in cytoplasmic puncta of KSHV infected
674 cells. Reactivated and unreactivated BAC16.iSLK and TREx-BCBL1 cells were stained with
675 antibodies to ORF68 (red), the viral replication compartment marker ORF59 (green), and DAPI
676 (blue). The far-right panel shows the merged image.

677

678 **Figure 3**

679 Characterization of the ORF68-deficient (ORF68^{PTC}) mutant virus. (A) Diagram depicting the
680 genetic locus of ORF68 and the mutations inserted into the ORF68^{PTC} virus. (B) Western blots
681 showing expression of the early ORF59 protein and the late K8.1 protein in WT, ORF68^{PTC}, and
682 ORF68^{PTC}-MR viruses. Histone H3 served as a loading control. (C) DNA replication was measured

683 by qPCR of the viral genome before and after induction of the lytic cycle. (D) Progeny virion
684 production was assayed by supernatant transfer and flow cytometry of target cells.
685
686 **Figure 4**
687 ORF68^{PTC} virus displays a genome cleavage defect. (A) Diagram depicting the DNA cleavage
688 assay protocol and the expected TR DNA laddering phenotype (or lack thereof) upon infection
689 with WT or ORF68^{PTC} virus. (B) Southern blot of the PstI-HF digested DNA with a TR probe from
690 cells infected with WT, ORF68^{PTC}, or ORF68^{PTC}-MR virus.
691
692 **Figure 5**
693 Transmission electron microscopy of WT and ORF68^{PTC} KSHV-infected cells. (A) Representative
694 images of the nuclei of iSLK cells infected with WT or ORF68^{PTC} KSHV. Boxed regions are shown
695 to the right at higher magnification to better visualize virion morphology. (B) Representative
696 images of individual capsids observed in iSLK cells infected with WT or ORF68^{PTC} KSHV, grouped
697 by their maturation stage. Only B-capsids were observed in cells infected with ORF68^{PTC} KSHV.
698
699 **Figure 6**
700 Purification of recombinant ORF68 from transiently transfected HEK293T cells. (A) Collodial
701 coomassie-stained gel demonstrating the purity and molecular weight (~52 kDa) of ORF68
702 eluted from the s200 gel filtration column. Fractions containing ORF68 were pooled,
703 concentrated, and dialyzed into storage buffer; a sample of which was loaded in the final lane.

704 (B) Absorbance trace of the s200 gel filtration column, measured at 280 nm. The first peak
705 represents the void elution at 45.52 ml and the second peak represents ORF68 at 60.35 ml.
706
707 **Figure 7**
708 Purified recombinant ORF68 shows robust DNA binding and is associated with nuclease activity.
709 (A) Representative EMSA showing increasing amounts of ORF68 binding to the subunit-length
710 TR DNA probe. (B) Binding curve of ORF68 to DNA derived from quantification of three
711 technical replicates of the EMSA, yielding an observed K_d of (53.34 ± 2.11) nM with a Hill
712 coefficient of 1.88 ± 0.12. (C) Nuclease assay with increasing amounts of ORF68, incubated with
713 an ~800bp TR probe in the presence or absence of EDTA. (D) Analysis of TR probe degradation
714 in the presence of purified ORF68 upon addition of the indicated metal. (E) Gel comparing
715 degradation of the TR probe in the presence of purified ORF68 or DNaseI +/- 1mM TPEN or 50
716 mM EDTA.

Figure 1

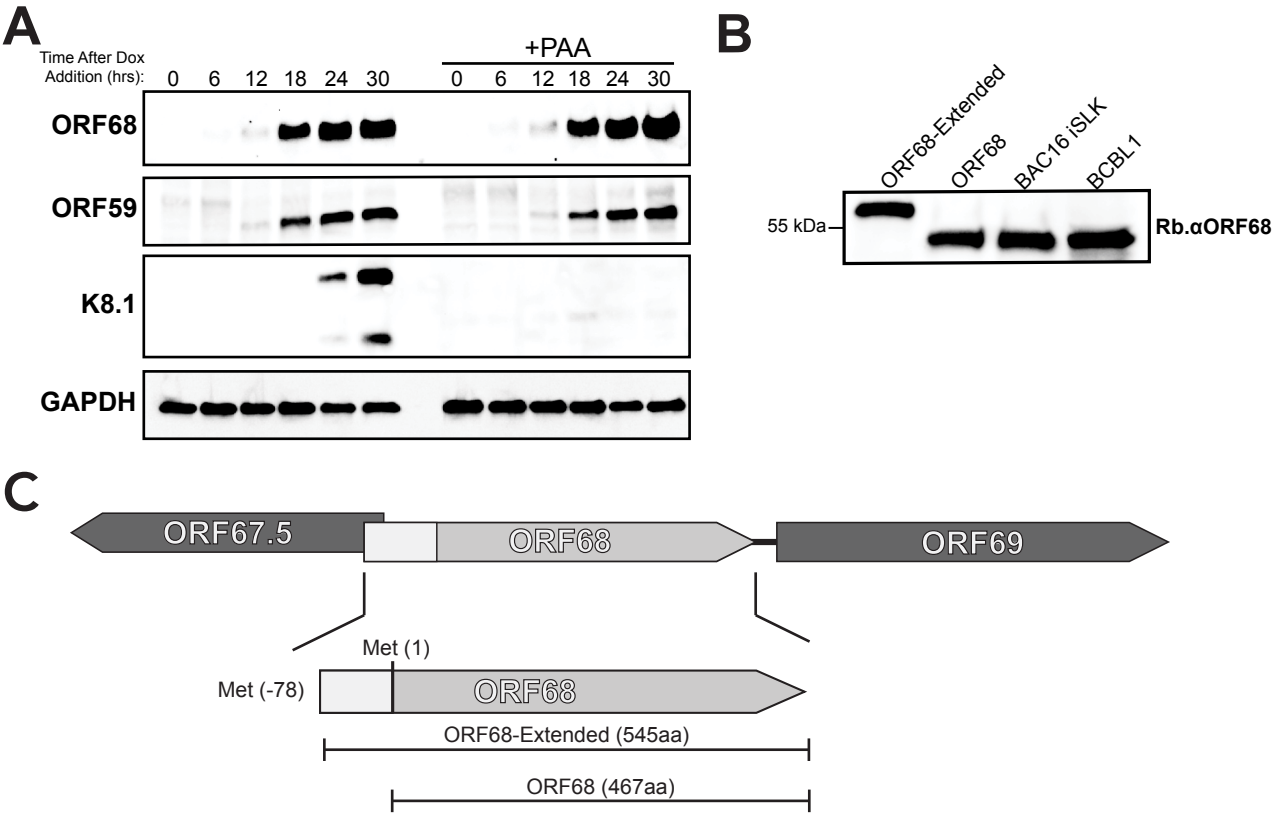
A
Time After Dox Addition (hrs):
0 6 12 18 24 30
+PAA
0 6 12 18 24 30
ORF68
ORF59
K8.1
GAPDH
B
ORF68-Extended
ORF68
BAC16 iSLK
BCBL1
55 kDa
Rb.αORF68
C
ORF67.5
ORF68
ORF69
Met (1)
Met (-78)
ORF68
ORF68-Extended (545aa)
ORF68 (467aa)

Figure 2

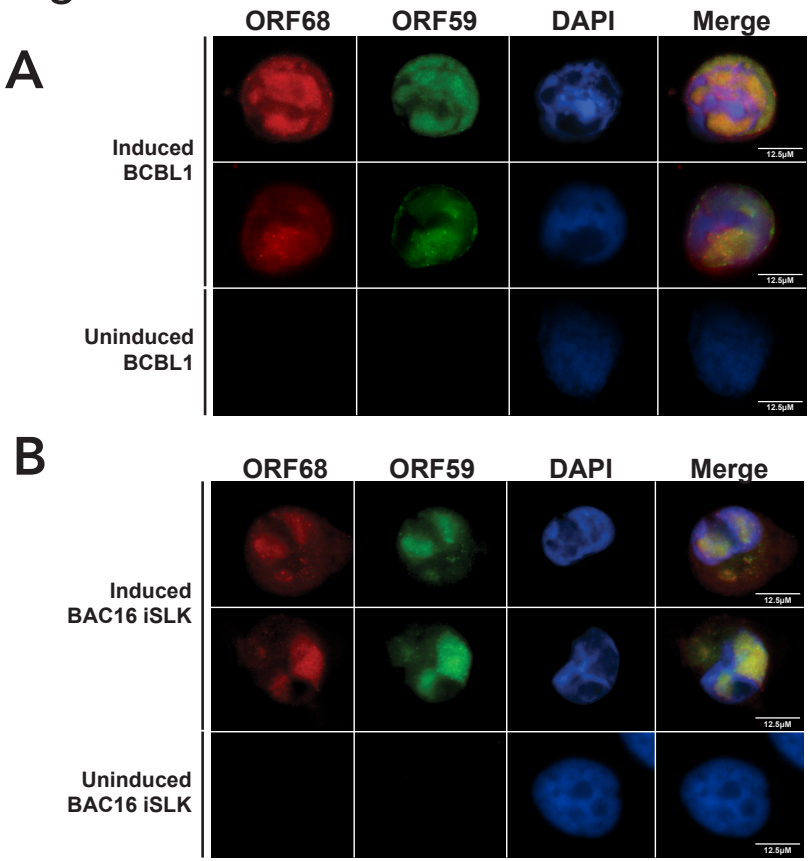
A
ORF68
ORF59
DAPI
Merge
Induced BCBL1
Uninduced BCBL1
12.5μM
B
ORF68
ORF59
DAPI
Merge
Induced BAC16 iSLK
Uninduced BAC16 iSLK
12.5μM

Figure 3

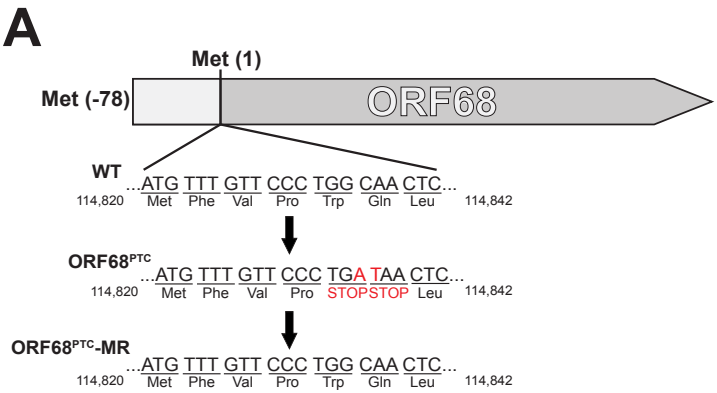
A
Met (1)
Met (-78)
ORF68
WT
...ATG TTT GTT CCC TGG CAA CTC...
114,820 Met Phe Val Pro Trp Gln Leu 114,842
ORF68PTC
...ATG TTT GTT CCC TGA TAA CTC...
114,820 Met Phe Val Pro STOPSTOP Leu 114,842
ORF68PTC-MR
...ATG TTT GTT CCC TGG CAA CTC...
114,820 Met Phe Val Pro Trp Gln Leu 114,842

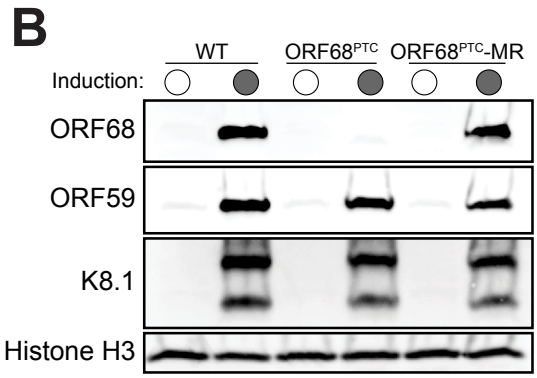
B
WT
ORF68PTC
ORF68PTC-MR
Induction:
ORF68
ORF59
K8.1
Histone H3

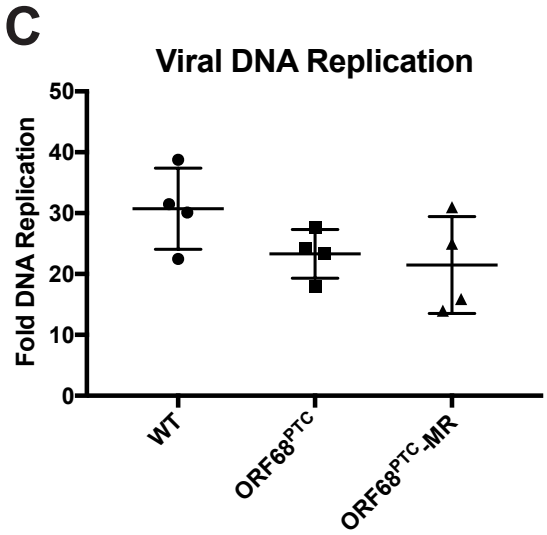
C
Viral DNA Replication
Fold DNA Replication
50
40
30
20
10
0
WT
ORF68PTC
ORF68PTC-MR

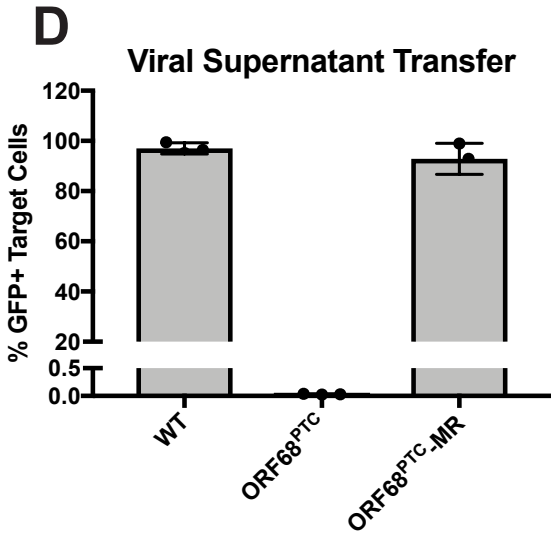
D
Viral Supernatant Transfer
% GFP+ Target Cells
120
100
80
60
40
20
0.5
0.0
WT
ORF68PTC
ORF68PTC-MR

Figure 4

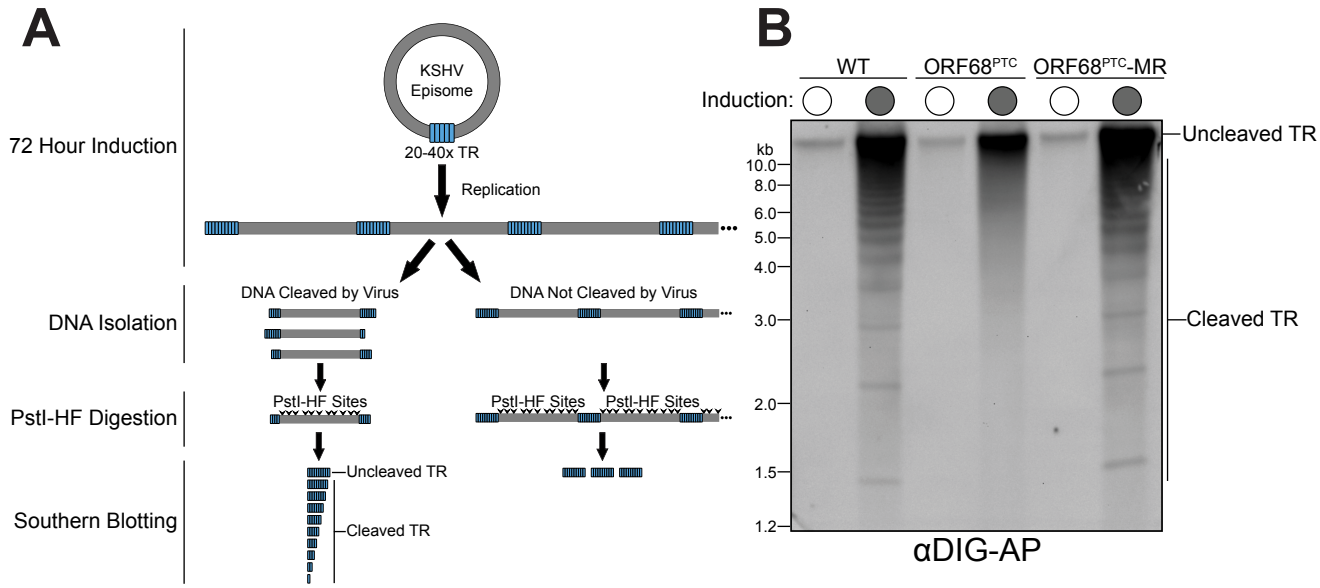
A
72 Hour Induction
KSHV Episome
20-40x TR
Replication
DNA Isolation
DNA Cleaved by Virus
DNA Not Cleaved by Virus
PstI-HF Digestion
PstI-HF Sites
PstI-HF Sites
PstI-HF Sites
Southern Blotting
Uncleaved TR
Cleaved TR
B
WT
ORF68PTC
ORF68PTC-MR
Induction:
kb
10.0
8.0
6.0
5.0
4.0
3.0
2.0
1.5
1.2
Uncleaved TR
Cleaved TR
αDIG-AP

Figure 5

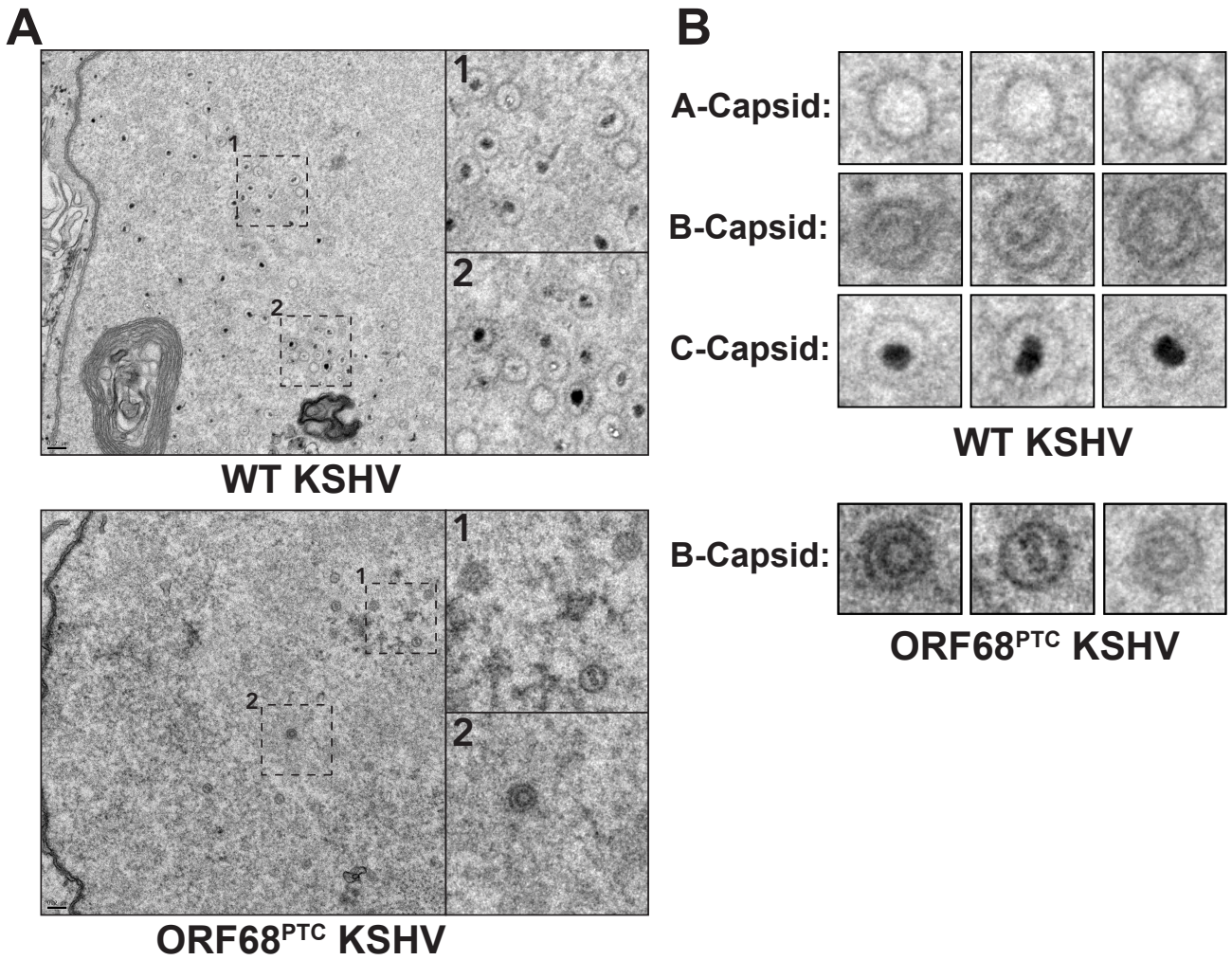
A
1
2
WT KSHV
ORF68PTC KSHV
B
A-Capsid:
B-Capsid:
C-Capsid:
WT KSHV
B-Capsid:
ORF68PTC KSHV

Figure 6

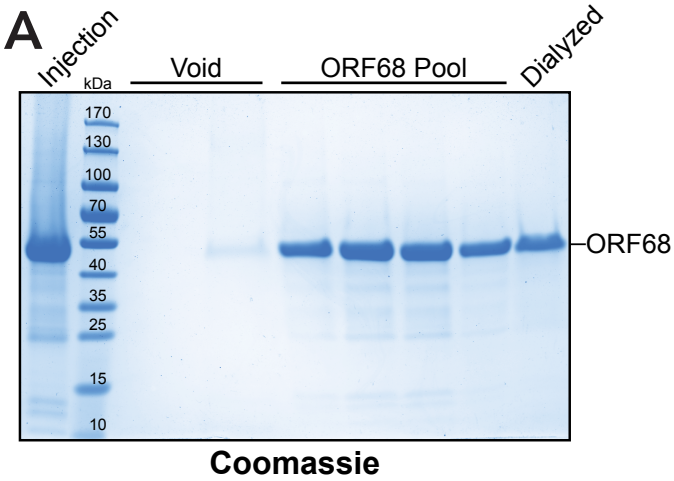
A
Injection
Void
ORF68 Pool
Dialyzed
kDa
170
130
100
70
55
40
35
25
15
10
ORF68
Coomassie

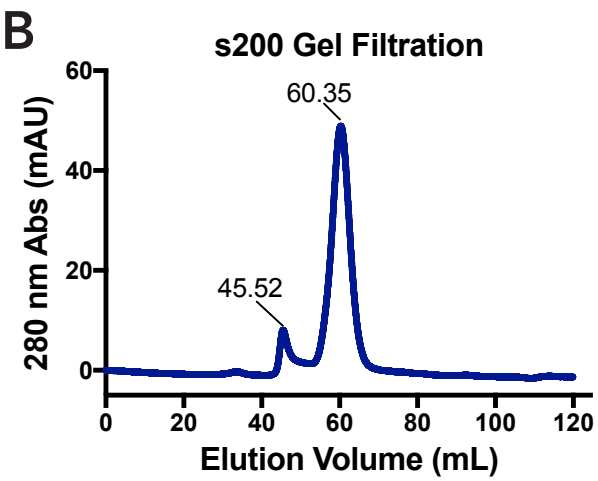
B
s200 Gel Filtration
60.35
45.52
280 nm Abs (mAU)
60
40
20
0
0
20
40
60
80
100
120
Elution Volume (mL)

Figure 7

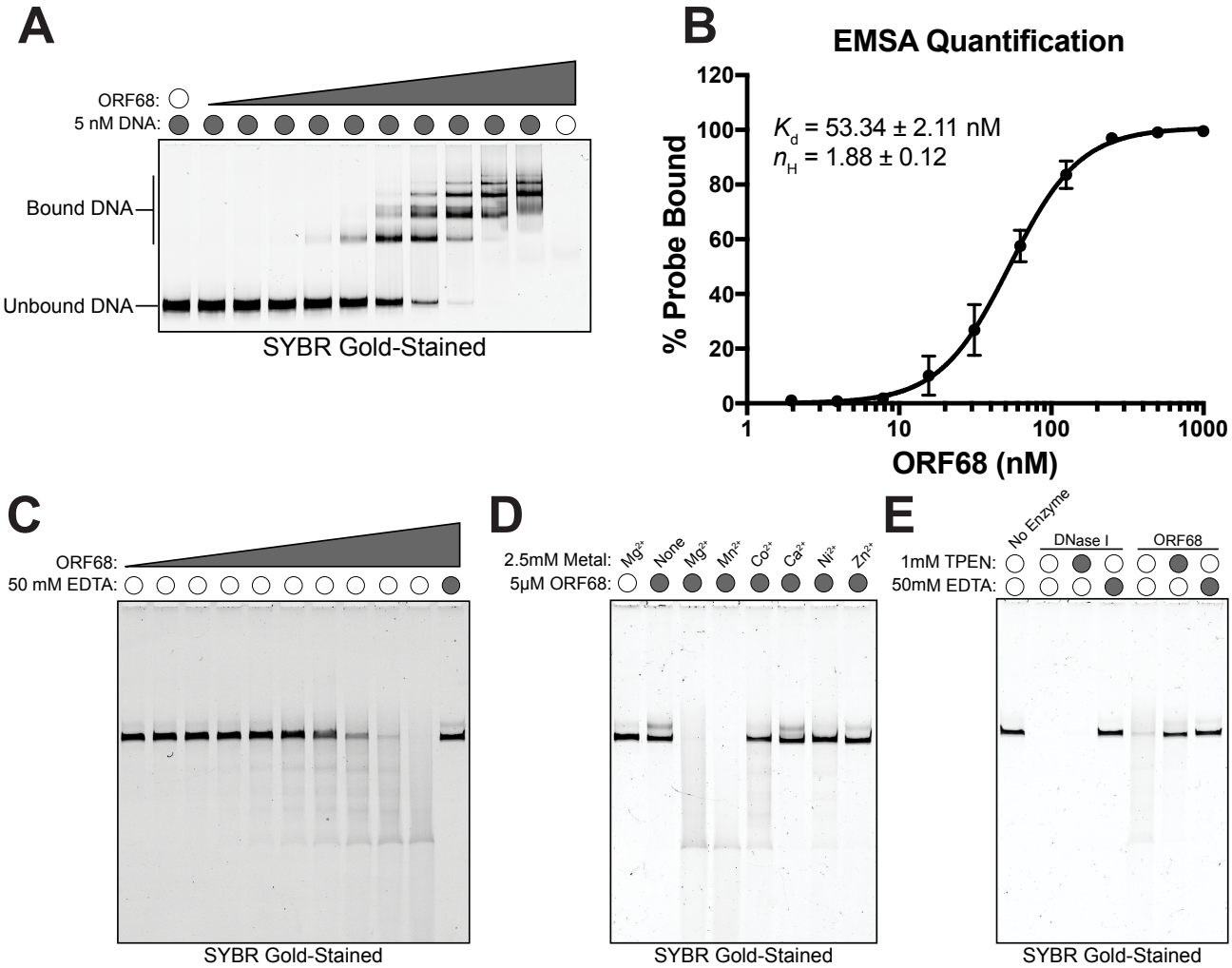
A
ORF68:
5 nM DNA:
Bound DNA
Unbound DNA
SYBR Gold-Stained
B
EMSA Quantification
K_d = 53.34 ± 2.11 nM
n_H = 1.88 ± 0.12
% Probe Bound
ORF68 (nM)
C
ORF68:
50 mM EDTA:
SYBR Gold-Stained
D
2.5mM Metal:
5μM ORF68:
Mg^{2+}
None
Mg^{2+}
Mn^{2+}
Co^{2+}
Ca^{2+}
Ni^{2+}
Zn^{2+}
SYBR Gold-Stained
E
No Enzyme
DNase I
ORF68
1mM TPEN:
50mM EDTA:
SYBR Gold-Stained